Electronic structure and chemical and magnetic interactions in ZnO doped with Co and Al: Experiments and *ab initio* density-functional calculations

Diana Iuşan,* Ronny Knut, Biplab Sanyal, Olof Karis, and Olle Eriksson
Department of Physics and Materials Science, Uppsala University, Box 530, SE-75121, Uppsala, Sweden

Victoria A. Coleman and Gunnar Westin
Department of Materials Chemistry, Uppsala University, Box 538, SE-75121, Uppsala, Sweden

J. Magnus Wikberg and Peter Svedlindh
Department of Engineering Sciences, Uppsala University, Box 534, SE-75121, Uppsala, Sweden
(Received 19 April 2008; published 25 August 2008)

We present results of electronic structure and magnetization measurements of Co:ZnO and Co:ZnO codoped with Al thin-film samples fabricated by solution-based methods together with *ab initio* electronic structure calculations. Electronic structure measurements indicate that the Co states lie close to the valence-band edge with pinning of the Fermi level primarily due to native defects yielding a heavily *n*-doped material. The findings in the electronic structure measurements are corroborated by results from theoretical calculations. We find that it is necessary to go beyond the local-density approximation to achieve agreement with experiments. Moreover, the theoretical calculations indicate a tendency for the formation of Co clusters, giving rise to an antiferromagnetic exchange interaction between the Co atoms. The magnetization measurements are well in line with the theoretical predictions, showing a dominating superparamagnetic behavior arising from small antiferromagnetic clusters containing uncompensated spins.

DOI: 10.1103/PhysRevB.78.085319 PACS number(s): 75.50.Pp, 75.70.−i, 71.70.Gm, 78.70.Dm

I. INTRODUCTION

The possibility to manipulate the spin of the electron, as well as the charge, opens up fascinating routes for processing information and data storage. This is particularly exciting in terms of semiconductor spintronics, where conventional charge-based electronics could be replaced with devices possessing both spin and charge functionality. By doping a transition metal (TM) into a semiconducting material, one hopes to achieve a ferromagnetic semiconductor—a so-called diluted magnetic semiconductor (DMS)—which is operational at room temperature (RT). A prototype example of such a DMS material is Mn-doped GaAs for which a ferromagnetic transition temperature of around 173 K (Ref. 1) has been achieved. As the concentration of the magnetic dopants in III-V semiconductors is believed to be limited to around 10%, considerable attention has moved to TM-doped II-VI DMS materials. A special interest has been drawn to TM-doped ZnO as a possible DMS material due to the existence of a number of theoretical[2–4] and experimental reports of ferromagnetism above RT for these materials.[5–14] ZnO is also highly relevant from an application perspective as the material is piezoelectric, optically transparent, and has a large band gap of 3.4 eV. For the Co-doped ZnO system, the expected ferromagnetic (FM) ordering was predicted to be due to double exchange interactions between the Co ions.[4]

Despite initial intriguing results, reports on Co:ZnO have been very inconclusive even when seemingly identical material prepared by the same methods has been used. A large deviation between results is reported, ranging from very high magnetic moments [(6 to 0.01 μ_B/Co with a T_C above 300 K (Ref. 15)] to the absence of ferromagnetic behavior down to cryogenic temperatures.[16] Several attempts have been made to explain the origin of the observed magnetic behavior (see, e.g., Refs. 6, 7, 9, and 17); however, much controversy still remains regarding the intrinsic magnetism in TM-doped ZnO. The FM behavior has been explained to be carrier mediated,[11,18] although this conclusion has been questioned by some authors.[10,19,20]

The consensus today is that the magnetic properties of TM-doped ZnO strongly depend on defects as well as on the chemical configuration of the dopants. Some of us have already shown[21] that the clustering tendency of Co atoms brings inhomogeneity that strongly affects the magnetization. Depending on the concentration of Co atoms, one may get an increase or a decrease in the Curie temperature. This is an extremely important point in the context of nanoscale phase separation in DMS.[22–24] It should be mentioned that a superparamagnetic phase occurring due to nanoscale clusters can easily be misinterpreted as intrinsic ferromagnetism. Concerning defects, it was recently shown that although the magnetic interaction between Co atoms is extremely short ranged in defect-free ZnO, the presence of oxygen vacancies (O_{vac}) forming Co-O_{vac} pairs gives longer ranged interactions and, hence, a sizable Curie temperature.[25] Usually ZnO is intrinsically an *n*-type semiconductor due to the presence of O_{vac}. Carrier-mediated ferromagnetism is likely to play an important role in achieving DMS ZnO. Thus by increasing the available charge carriers in ZnO, for example, with a known electron donor such as Al,[26] it may be possible to improve the ferromagnetic properties of the host material. Very recently, such a study has been conducted[10] where the authors demonstrated ferromagnetism in insulating and metallic films of different carrier concentrations. It was reported that the effective magnetic moment first increased and then decreased as a function of the ratio of the density of carriers to

that of the magnetic ions with a maximum effective moment at around a ratio of 0.4.

The aim of this work is to thoroughly study the electronic structure, chemical, and magnetic interactions in Co-doped, as well as Co- and Al-doped ZnO thin films, using a combination of *ab initio* density-functional calculations and experiments. Samples were fabricated by spin-coating acetate-based precursors on Si/SiO_2 substrates and were experimentally characterized with respect to microstructure, electronic structure, and magnetic properties. Also, theoretical calculations of the influence of chemical disorder and Al codoping on the magnetic properties have been performed.

II. EXPERIMENTAL DETAILS

The samples used in this study were 5% Co:ZnO and 5% Co,0.8% Al:ZnO fabricated on Si substrates via solution-based methods. To form the films, 0.25 M (metal concentration) solutions of zinc acetate dihydrate, cobalt acetate tetrahydrate, and aluminum nitrate dissolved in methoxyethanol were synthesized. Ethanolamine was used to stabilize the cobalt and zinc precursor solutions in a 1:1 ratio with the metal ions. The precursor solutions were then mixed to obtain either a 5% Co:ZnO or a 5% Co,0.8% Al:ZnO solution, which was subsequently spin coated on clean Si/SiO_2 wafers (3000 rpm at 40 s). After each coat, the films were heated at 600 °C for 10 min in air atmosphere. This process was repeated ten times to yield a homogeneous dense film with a total thickness of 110 nm. A final heat treatment in air at 600 °C or alternatively at 800 °C for 1 h was then performed. The surface morphology and crystal microstructure of the resultant films were monitored with scanning electron microscopy (SEM) (LEO 1440 at 3 keV) and grazing incidence (GI) x-ray diffraction (XRD) (GI-XRD) (3° in Siemens D5000 diffractometer with parallel-plate geometry).

Electronic structure measurements were performed on beamline D1011 at the Swedish synchrotron facility MAX lab. This bending magnet beamline comprises a plane grating monochromator (modified Zeiss SX-700) and end stations for photoelectron spectroscopy (PES) and x-ray absorption spectroscopy (XAS).[27,28] By a local alteration of the electron orbit x-rays with partially circular polarization are obtained. This enables element specific magnetic investigations using the x-ray magnetic circular dichroism technique (XMCD). The samples were mounted with Cu clips on a Cu holder to ensure good electrical contact between the sample and holder. No influence of sample charging effects was observed at any time during measurement. Prior to all measurements, the samples were heated to 230 °C for 15 min at a base pressure of 5×10^{-10} Torr to remove physisorbed contaminants. XAS at the Co $2p$ edges was recorded in total electron yield mode and the incident-beam current I_0 was monitored on a clean Au grid. The samples were held normal to the incident beam for the XAS and PES measurements, while several incidence angles were explored for the XMCD measurement. The XAS spectra were corrected by I_0 and pre-edge normalized before a linear background was subtracted. Finally, the spectra were normalized at high energies to represent the absorption on a "per atom" basis. PES and resonant photoelectron spectroscopy (RPES) were recorded using a 200-mm-radius hemispherical electron energy analyzer of Scienta type.[29] Additional photoelectron measurements were performed at the BESSY synchrotron in Berlin on the KMC-1 beamline at the high kinetic energy photoemission (HIKE) end station.[30]

dc magnetic measurements were performed in a Quantum Design magnetic property measurement system (MPMS-XL) superconducting quantum interference device (SQUID) magnetometer. Magnetization (M) vs temperature (T) measurements were performed between 2 and 375 K, applying a field (H) of 500 Oe and subsequent M vs H measurements were performed at 2 K between 30 and −30 kOe.

III. COMPUTATIONAL DETAILS

Two different methods have been considered for the electronic structure calculations using density-functional theory within the local spin-density approximation (LSDA) or generalized gradient approximation. Both approximations for the treatment of exchange-correlation potential yield the same result. In the supercell approach, the calculations have been performed using a plane-wave basis within the projector augmented-wave method[31] as implemented in the VASP package.[32] The LSDA+U method[33] has been used with the Coulomb interaction parameters $U=9$ and 5 eV for the d electrons of Zn and Co atoms, respectively. The exchange parameter J has been set to 1 eV. The wave functions were expanded in a plane-wave basis set with the kinetic energy cutoff of 500 eV. A Γ-centered $3\times3\times2$ $\boldsymbol{k}$-points mesh has been used in the Monkhorst-Pack scheme. We have used a $3a\times3a\times3c$ wurtzite supercell of 108 atoms in which three/one of the Zn sites were substituted by Co or Al atoms, respectively. The geometry of the systems was optimized until the force components were less than 0.01 eV/Å.

For the calculations of the chemical and magnetic pair interactions, we have used the Green's function Korringa-Kohn-Rostoker (KKR) method[34] within the atomic sphere approximation (ASA). LSDA was used along with an *spdf* basis. In order to treat the disorder, the coherent-potential approximation (CPA) has been employed. The magnetic pair-exchange parameters of a classical Heisenberg model have been calculated using the methodology of Liechtenstein *et al.*[35] employing the magnetic force theorem. The expression for evaluating the Heisenberg pair-exchange parameter is the following:

$$J_{ij}=\frac{1}{4\pi}\int^{E_F} dE\ \mathrm{Im}\ \mathrm{Tr}_L(\Delta_i T_{\uparrow}^{ij}\Delta_j T_{\downarrow}^{ji}), \tag{1}$$

where $\Delta_i=t_{i\uparrow}^{-1}-t_{i\downarrow}^{-1}$ and t being the on-site scattering matrix. T is the scattering path operator, which requires the calculation of the off-diagonal element of the Green's function. Tr_L indicates the trace over the orbital indices of the scattering matrices. A positive (negative) J_{ij} corresponds to a ferromagnetic (antiferromagnetic) interaction. The use of a classical Heisenberg model for the present system is valid as the magnetic moment of Co is large and rigid. This methodology has been applied successfully to different magnetic systems in

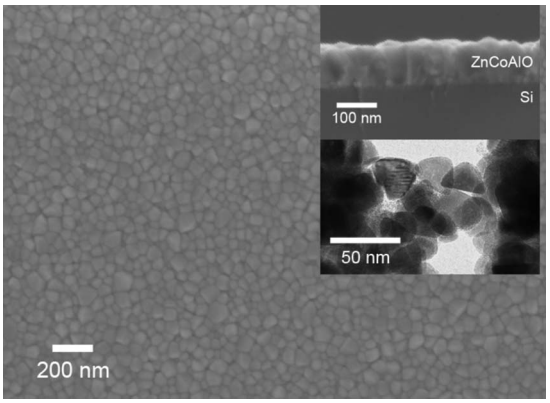

FIG. 1. SEM image of a typical 5% Co:ZnO film annealed in air at 800 °C for one hour. The inset on the top right shows a corresponding cross-sectional SEM image of the film. It can be noted that the film is polycrystalline and dense. The lower inset in the figure shows a TEM image taken from 5% Co:ZnO powder annealed at 500 °C. The uniform crystal shape and size indicate that the samples are homogeneous and appear phase pure.

the past.[36–38] The chemical pair interactions have been evaluated using the generalized perturbation method.[39] The effective chemical pair interaction parameters can be calculated as

$$\tilde{V}_{ij} = V_{ij}^{\text{Co-Co}} - 2V_{ij}^{\text{Co-Zn}} + V_{ij}^{\text{Zn-Zn}}, \quad (2)$$

where $V_{ij}^{\alpha\beta}$ is the interaction when sites i and j are occupied by α and β atoms, respectively. A positive (negative) V_{ij} indicates a repulsive (attractive) chemical interaction.

IV. RESULTS AND DISCUSSION

A. Structural characterization

Figure 1 shows a typical SEM image as obtained from the thin-film samples. The films are uniform, dense, and polycrystalline with an approximate grain size of 40 nm. The top left inset of the figure shows a corresponding cross-sectional SEM image of one film, again illustrating that the films are dense all the way down to the substrate. The thickness of the films is determined to be 110 ± 10 nm. The cross-sectional image also suggests that the polycrystalline grains possess some columnar character, which may be indicative of a preferential growth direction, an observation that is further substantiated by our XRD investigations (see below). The lower inset in Fig. 1 shows a TEM image of the 5% Co:ZnO precursor solution heated to 500 °C. This image shows particles of uniform size and shape suggesting a homogeneous phase pure material.

The phase purity and high crystalline quality of the films are further confirmed by XRD studies shown in Fig. 2. This figure shows GI (3°) XRD patterns from 5% Co:ZnO and 5% Co and 0.8% Al:ZnO films annealed at 800 °C in air, along with the reflections from pure ZnO powder for reference. Both films possess strong ZnO reflections and do not show any intensity at other angles confirming that the samples are phase pure. Furthermore, the reflections at 36° and 63° are enhanced with respect to the relative intensities

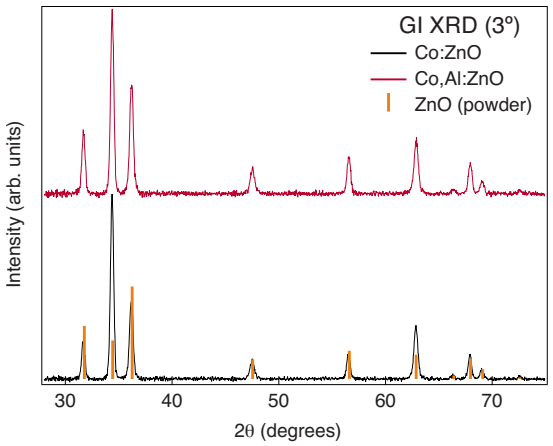

FIG. 2. (Color online) GI (3°) XRD scans of 5% Co:ZnO and 5% Co, 0.8% Al:ZnO films grown on Si and annealed at 800 °C. Bars indicating the random orientation diffraction pattern expected from pure ZnO is shown as a reference. In both samples, only reflections originating from ZnO can be seen, indicating that both films are phase pure. Additionally, there is evidence of some preferential c axis texturing in the samples with the reflections at 36° and 63° showing enhanced intensity compared to the relative intensities expected from an entirely random sample. This observation is further supported by the SEM results in Fig. 1.

expected from a randomly oriented sample, i.e., the powder sample. These reflections correspond to c-axis reflections suggesting that there is preferential growth occurring along the c axis in the films. We note here that Co:ZnO samples with higher Co content ($\gtrsim$7%) were also investigated and evidence of a secondary $(Zn,Co)_3O_4$ spinel phase was found. We emphasize that no evidence of a secondary phase is found within the detection limits of our XRD measurements nor from the electronic structure measurements described below at the Co concentration (5%) used in this study.

B. Electronic structure

In Fig. 3 we show the Co $L_{2,3}$ absorption spectra for Co:ZnO and Co,Al:ZnO. The multiplet structure of the peaks is a clear indication that the Co is not in a metallic state. The spectra are similar to other results reported in the literature,[40–42] which have been shown to correspond to Co 2+ states in tetrahedral coordination,[40,42] indicating Zn substitution. XMCD measurements (not shown) were performed in remanence after pulsing the samples in plane with a 0.1 T field at the Co $L_{2,3}$ edge for several angles and temperatures (RT and 100 K). For all samples, the XMCD data showed no indication of ferromagnetically ordered Co moments.

Figure 4 shows PES results for the Co 2p core states measured on the KMC-1 beamline BESSY in Berlin (Germany). To increase the bulk sensitivity, a photon energy of 3 keV was used. This results in a kinetic energy of approximately 2.2 keV at which the electron mean path is around 3 nm, implying a total probe depth in the range of 10 nm. The total-energy resolution for these measurements was 400 meV. The shape of the spectrum is very similar to that of

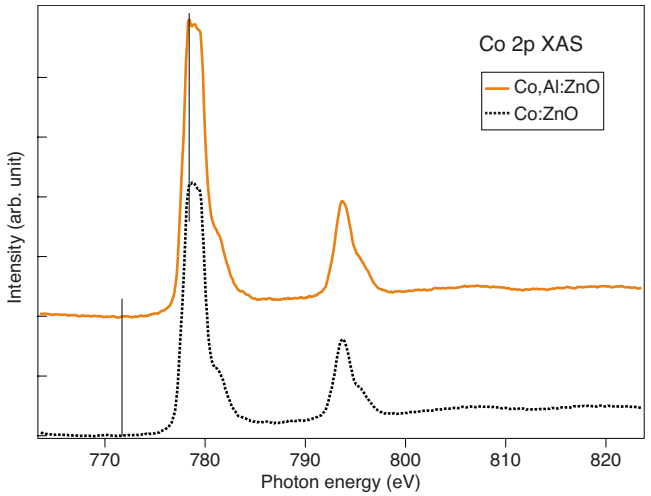

FIG. 3. (Color online) Absorption spectra of Co $L_{2,3}$ edges for Co:ZnO and Co,Al:ZnO. The two spectra are very similar and no energy shift is observed between the two samples. Both spectra exhibit typical multiplet features for Co in a 2+ electronic configuration and correspond well to other results reported in the literature (Refs. 40–42). The vertical lines indicate the excitation energies used for the resonant photoemission measurements (see text and Fig. 5).

CoO (Refs. 40 and 43–45), supporting the XRD and XAS results indicating phase pure samples. The valence band (VB) of CoO is mainly comprised of an admixture of Co d^7 and d^8L states, where L is a hole in the oxygen $2p$ band. Due to this hybridization, photoemission of the spin-orbit split Co $2p$ results in both $2p^5 3d^7$ and $2p^5 3d^8 L$ final states. The

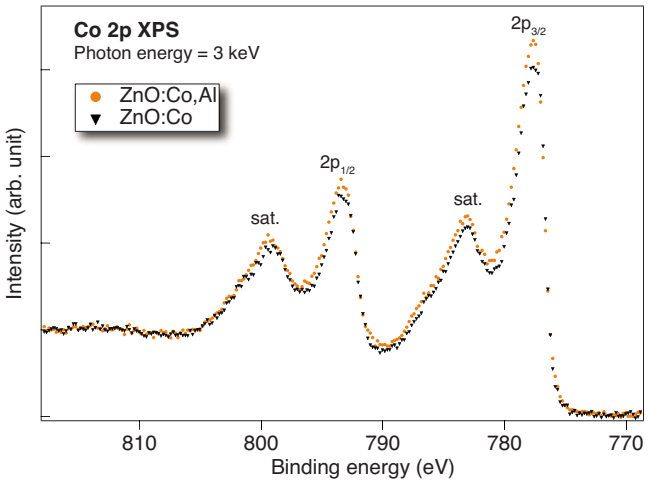

FIG. 4. (Color online) Core-level XPS spectra of the spin-orbit split Co $2p$ level. A photon energy of 3 keV was used to obtain increased bulk sensitivity. The main peaks and the satellites are due to different final states of core-hole excited Co hybridizing with O $2p$ and is thus a signature of the electron correlation in the doped ZnO. The main peaks are due to $2p^5 3d^8 L$, where L is a hole in the oxygen $2p$ band and the satellites are due to $2p^5 3d^7$ final states (Refs. 43 and 44). The spectra are very similar to that of CoO (Refs. 40 and 43–45), which indicates substituted Co in a 2+ ionic state.

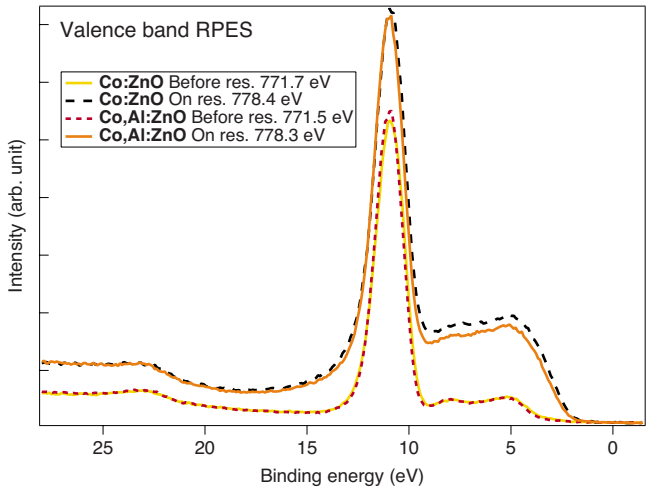

FIG. 5. (Color online) On- (dashed) and off- (solid and dotted) resonances PES for Co:ZnO and Co,Al:ZnO. The excitation energies around the Co $2p_{3/2}$ edge are marked in Fig. 3. The strong resonant enhancement at the VB edge is due to Co $3d$ states filling the core hole and is thus a signature of the partial Co $3d$ DOS.

main lines have been shown to correspond to $2p^5 3d^8 L$ final-state electronic configurations while the satellites are due to $2p^5 3d^7$ final states.[43,44]

VB RPES for Co:ZnO and Co,Al:ZnO are shown in Fig. 5 and were recorded with the on-resonance (~778 eV) and off-resonance (~772 eV) energies marked in Fig. 3. With photon energies at the Co L_3 absorption maximum, photoemission is resonantly enhanced due to de-excitation of Co $2p$ core-hole states resulting in one and two-hole final states in the Co $3d$ states. The strong resonant enhancement at ~2.5 eV is thus a signature of Co $3d$ states at the VB edge.

The corresponding high-resolution VB PES spectra are shown in Fig. 6 for ZnO, Co:ZnO, Al:ZnO, and Co,Al:ZnO. The spectra were recorded with 200 eV photon energy and with a total-energy resolution of 200 meV. The binding energies are referred to the Fermi level of a clean Cu sample holder, which is in electrical contact with the samples. The large peak at 11 eV binding energy is assigned to Zn $3d$ states, while the states near the band edge are mainly O $2p$ and O-Co p-d hybridized states.

The outermost part of the VB recorded with high statistics and the corresponding difference spectra between samples with and without Co doping are shown in Figs. 7(a) and 7(b), respectively. The difference spectra in Fig. 7(b) can be regarded as a partial density of states (PDOS) for Co if the hybridization with the ZnO host is not too strong.[46] According to the difference spectra, the Co states are located at the VB edge (~3 eV) and around a binding energy of 7 eV. This is also confirmed by RPES (see Fig. 5) where a strong resonant enhancement is found in this energy range. The negative PDOS at a binding energy of around 5 eV is due to a hybridization between Co and host ZnO states, which is not accounted for in our difference procedure.[46] Al codoping does not significantly influence the VB of ZnO but induces a clear modification of occupied Co states at the VB edge. The contribution of Co t_{2g} states appears to be narrower with Al

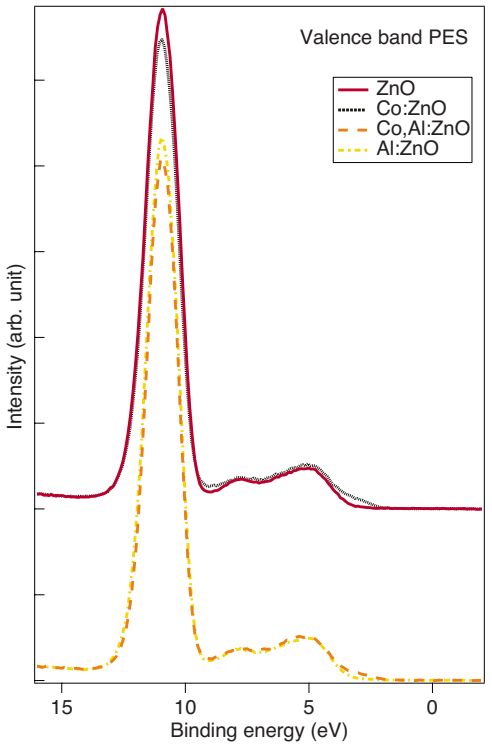

FIG. 6. (Color online) Valence-band spectra of ZnO and Co:ZnO (on top) and Al:ZnO and Co,Al:ZnO (bottom). The strong feature around 11 eV is the Zn 3*d* band. At lower binding energies, there are states primarily due to O 2*p* states and Co 3*d* states.

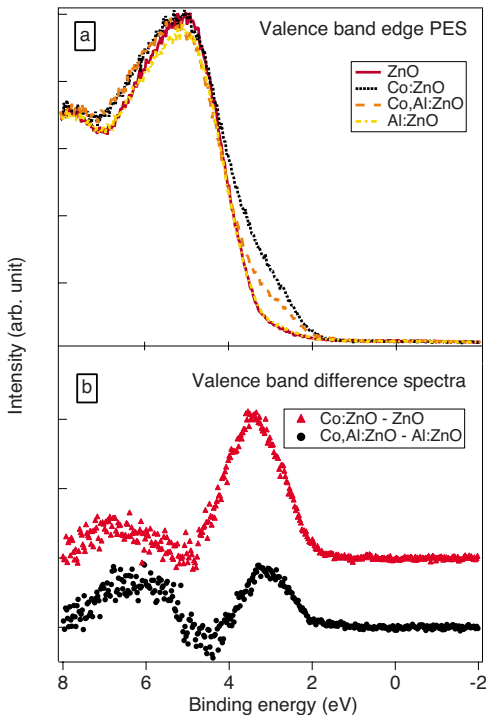

FIG. 7. (Color online) (a) VB edge PES of ZnO with and without Co and Al doping. There is no finite DOS at the Fermi level, indicating that the samples are semiconducting even though the chemical potential is located very close to the bottom of the conduction band (Fermi-level pinning). The addition of Al modifies the VB, an effect that is most visible at the VB edge. (b) Difference spectra between Co:ZnO–ZnO and Al,Co:ZnO–Al:ZnO. The distribution of Co states are mainly located at the top of the VB. Al codoping modifies the Co states yielding narrower Co t_{2g} states at the edge.

codoping indicating a more localized *d* band, an effect that is also observed in *ab initio* calculations shown below.

The tails at the VB edge are states due to inherent defects in the polycrystalline samples. Taking that in consideration, one finds that the binding energy of the VB edge for ZnO and Al:ZnO is similar to the band-gap size of crystalline ZnO of about 3.4 eV. Al acts as a shallow donor in ZnO and should therefore shift the position of the Fermi level located in the band gap. The similarity between the VB edge PES spectra of ZnO and Al:ZnO [cf. Fig. 7(a)] suggests that the Fermi energy is already located very close to the conduction band (pinned E_F) due to the large number of intrinsic defects creating highly *n*-doped samples. Since there is no finite DOS at the Fermi level, the samples can still to be considered as semiconducting.

The calculated DOS for pure and doped ZnO are shown in Figs. 8(a)–8(d). The VB consists mainly of O 2*p* states and has a width of approximately 5 eV. The Zn 3*d* states are localized in energy at roughly 8 eV below the VB maximum, which is in agreement with the experiment. We have used a *U* value on the Zn 3*d* states to shift the states to higher binding energy to achieve agreement with experiments. An equally important point to be noted here is the position of the Co *d* states. Calculations based on LDA produce Co *d* states in the gap of ZnO, whereas LDA+*U* calculations with *U* on Co shifts these states to the top of the VB. Using this latter method, we find that the location of the calculated Co *d* states to be in good agreement with the experimental results shown in Fig. 7. Similar findings have been reported by, e.g., Toyoda *et al.*[47] using self-interaction corrected local-density approximation.

The introduction of Al leads to a slight broadening of the Zn 3*d* states due to the hybridization to the Al states. Furthermore, the inclusion of Al in ZnO leads to a pinning of the Fermi level at the bottom of the conduction band, making the semiconductor *n* type.

The main peak in the DOS of Al is located ~1 eV below the bottom of the VB. As for the Co inclusion in ZnO, it brings up more states into the VB causing an increase in its width. The codoping of Co:ZnO with Al pushes the Co states down in energy with respect to the VB. By investigating Figs. 8(b) and 8(d), we can conclude that this is caused by the appearance of an extra peak in the Co DOS at the bottom of the VB.

C. Magnetic properties

For all measured samples, the *M* vs *T* measurements reveal a paramagnetic behavior with no sign of spin ordering even at the lowest temperatures investigated with an archetypical *M* vs *T* behavior shown in Fig. 9. A small difference in the magnetic response is observed with annealing at 800 °C yielding a somewhat higher magnetic moment (cf. inset of Fig. 9). With Al codoping, a small additional increase in the magnetic moment was seen—however—in con-

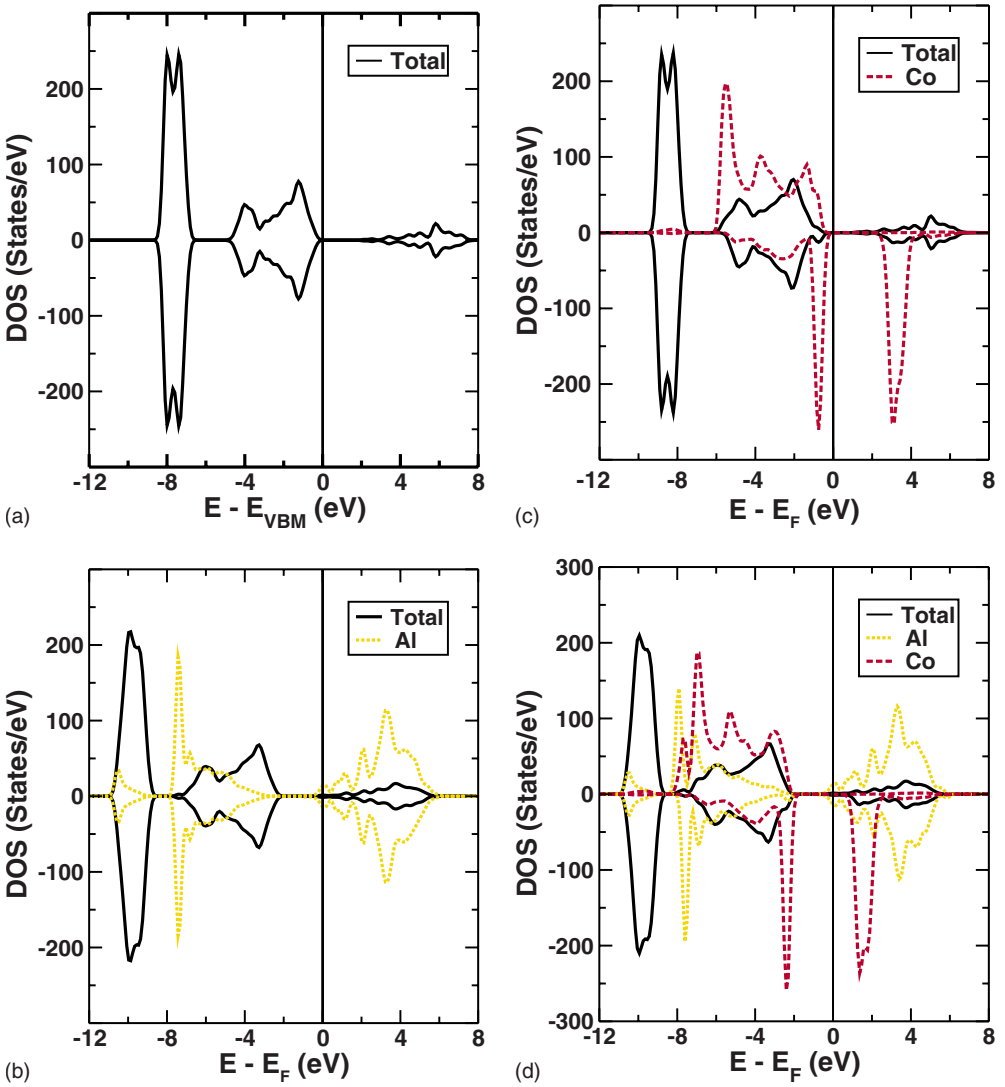

FIG. 8. (Color online) Calculated DOS for: (a) pure ZnO, (b) 1% Al:ZnO, (c) 5% Co:ZnO, and (d) 5% Co, 1% Al:ZnO. The Al and Co states are scaled.

trast to some expectations,[48] no hysteresis in the M vs H measurements was detected. Despite the absence of hysteresis, all samples exhibit an approach to saturation in the high-field region ($H \sim 30$ kOe), which is expected since the Zeeman and thermal energies are comparable in magnitude in the high-field region of our experiment at $T=2$ K (Fig. 10). In the case of Co-rich clusters that are either ferro/antiferromagnetically coupled with uncompensated spins in the latter case, the Zeeman energy will dominate over the thermal energy. From the low-field slope ($\chi = \partial M / \partial H$) of the M vs H curves, effective magnetic moments $\mu_{\text{eff}} = \sqrt{\chi \cdot 3k_B T / \mu_0 N_T}$ were extracted generating the results shown in Table I. N_T corresponds to the number of Co moments per unit volume and is obtained from $N_T = 2x / V_{\text{cell}}$, where x is the relative Co concentration and V_{cell} is the wurtzite cell volume. Additionally, Co magnetic moments $\mu_{\text{HF}} = M_s / N_T$ were extracted from the close to saturation magnetization value M_s measured at $H=30$ kOe. Comparing the μ_{eff} and μ_{HF} estimates, one notices that μ_{eff} in all cases gives the largest magnetic moment. Moreover, while μ_{eff} is

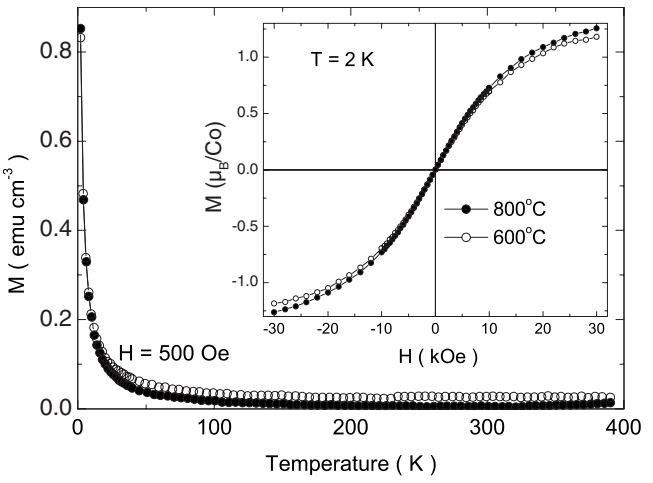

FIG. 9. Magnetization (M) vs temperature (T) and magnetization (M) vs field (H) (inset) for 5% Co:ZnO samples annealed in air for 1 h at 600 °C (open symbols) and 800 °C (filled symbols)

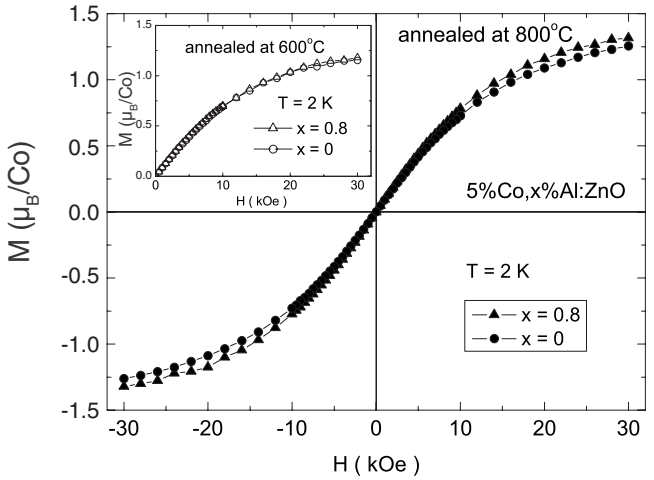

FIG. 10. Magnetization (M) vs field (H) for Co:ZnO samples with (triangles) and without (circles) Al codoping annealed in air for 1 h at 800 °C (filled symbols). The inset shows corresponding results for samples with (triangles) and without (circles) Al codoping annealed in air for 1 h at 600 °C (open symbols)

only slightly smaller in magnitude than the magnetic moment expected for localized Co in an ionic 2+ state (3 μ_B), μ_{HF} is considerably smaller. This is difficult to reconcile in a model with noninteracting atomic magnetic moments nor can it be explained in a superparamagnetic model assuming Co-rich clusters with ferromagnetically coupled magnetic moments. Instead, these results indicate the existence of antiferromagnetically coupled Co-rich clusters with uncompensated spins. From the proposal by Néel[49] in antiferromagnetic (AFM) nanoparticles, the uncompensated magnetic moments are proportional to n_c^q where n_c is the number of atomic moments in the cluster and $q=1/3$ or 1/2 for moments randomly distributed in the surface or in the volume, respectively. From this, a rough mean value for the number of Co spins present in each cluster can be estimated from the low-field magnetization $\chi=N_T/n_c^{1-2q}(\mu_0 m^2/3k_BT)$. In this expression m is the atomic Co magnetic moment, which according to theoretical results should take the value 3 μ_B. With these assumptions, using the experimental values for μ_{eff} and $q=1/3$, one arrives at $n_c \approx 3$. Using instead μ_{HF} to estimate n_c, one obtains from $M_s=N_T/n_c^{1-q}\cdot m$ values for n_c in the range of 4–6. One may argue that a power-law dependence of the cluster moment on cluster size does not hold for cluster sizes this small. However, other conceivable models will give similar results for μ_{eff} and μ_{HF} as long as there is more than one uncompensated spin in the cluster. The important result in this work is not the exact value of n_c. Instead, we would like to emphasize that the values obtained for μ_{eff} and μ_{HF} (μ_{HF} being smaller than both μ_{eff} and m) give a strong evidence for the existence of small Co-rich clusters containing uncompensated spins. The expressions above, involving a power-law dependence of the cluster moment on cluster size, can still be useful and give guidance when attempting to extract magnetic moments from magnetization curves especially in cases where the sample is expected to contain clusters several nanometers in size. In our samples, the small amount of Co spins present in each cluster will be very hard to detect with structural measurements. Also, if the clusters are coherently incorporated in the structure they will be almost invisible with standard high-resolutions techniques.[50]

TABLE I. $Co_{5\%}, Al_{x\%}$:ZnO for different annealing temperatures with magnetic moments from the high-field region (μ_{HF}) and the effective magnetic moments (μ_{eff}) derived from the low-field slope of the M vs H curves.

Annealing temp.	x	$\mu_{\mathrm{HF}}(\mu_B/\mathrm{Co})$	$\mu_{\mathrm{eff}}(\mu_B/\mathrm{Co})$	$\mu_{\mathrm{HF}}/\mu_{\mathrm{eff}}$
600 °C	0	1.15	2.69	0.43
600 °C	0.8	1.18	2.70	0.44
800 °C	0	1.25	2.75	0.45
800 °C	0.8	1.31	2.84	0.46

The absence of magnetic hysteresis (lack of remanence and coercive field), combined with a tendency for magnetic saturation at high applied fields and with an estimated value for μ_{HF} (well below the theoretical limit of 3 μ_B) strongly suggest that the dominating behavior is superparamagnetic. The observed superparamagnetic behavior is due to the formation of small antiferromagnetic clusters with uncompensated moments, yielding a net magnetic moment to each cluster.

In the paper by Behan *et al.*,[10] it has been shown that the carrier-concentration influences the effective magnetic moment of Co significantly. Based on this observation, the authors have argued that the carriers (electrons) mediate a Ruderman-Kittel-Kasuya-Yosida-type (ferromagnetic) exchange interaction, which results in an optimal ratio of free carriers to the number of magnetic ions, yielding an effective magnetic moment of about 1.6 μ_B per Co atom at optimal doping—corresponding to a heavily n-doped material. This moment is far from a saturation moment of 3 μ_B. We suggest that the observation made by Behan *et al.* is due to the presence of Co clusters of various sizes with uncompensated spins. The variation in the magnetic moment will then reflect the tendency to form clusters on the chemical potential and the presence of donor levels (or acceptor levels for p-type materials) in accordance with our calculations. Sufficiently large superparamagnetic clusters can result in a finite magnetic moment even at RT and can, thus, easily be misinterpreted as a ferromagnetic state. We thus propose that the variation of the magnetic moment on the carrier concentration is indirect and is only a consequence of the variation in cluster size distributions that follows as a direct consequence of the chemical composition.[22,50]

The calculated magnetic and chemical pair interactions within the CPA are shown in Figs. 11(a) and 11(b). The interactions are plotted as a function of Co-Co separation and for various Co concentrations, both in the presence and absence of Al. Typical to a TM-doped wide band-gap semiconductor, the interactions are short ranged and decay exponentially with Co-Co separation. The chemical interactions are negative indicating a tendency for clustering of the Co atoms. With Al codoping, they become more and more negative, signifying an even stronger tendency for clustering. Once again, we emphasize that the strong variation in the effective magnetic moment reported by Behan *et al.*,[10] could

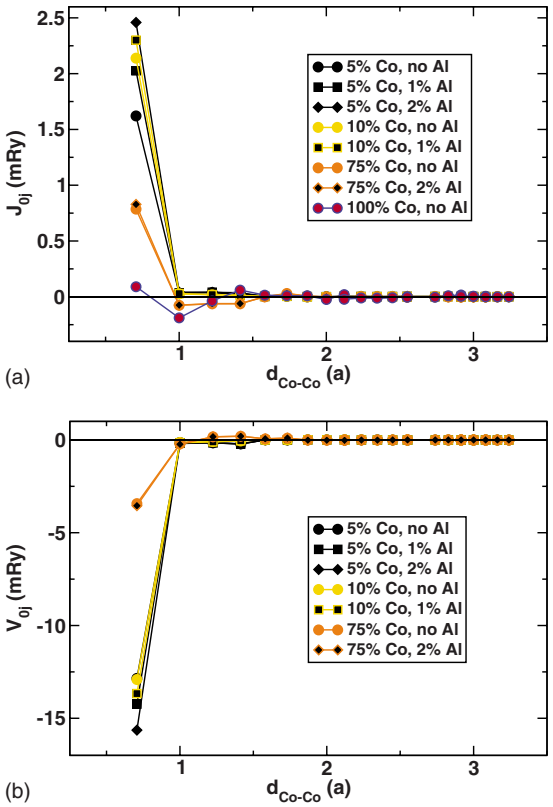

FIG. 11. (Color online) Calculated magnetic (a) and chemical (b) pair interactions versus Co-Co separation for different Co concentrations and in the presence and absence of Al_{Zn}.

be interpreted as being due to the increased tendency of cluster formation brought on by Al codoping and increased carrier concentration.

Concerning the magnetic interactions within Co:ZnO, they are ferromagnetic for low Co content (5%) but decrease for higher concentrations and turn out to be antiferromagnetic for very high Co content. The Al addition increases the strength of the interactions while keeping them short ranged.

Connecting the results for the chemical and magnetic interactions, we propose the following scenario for the magnetism of the system: For a low Co concentration and a random distribution of the atoms, the interactions are very localized in space. Due to the clustering tendency of the Co atoms further increased by Al codoping, we envision the formation of regions with high Co concentration for which the magnetic interactions among the Co atoms are antiferromagnetic. The calculated Curie temperature of the system is very low due to the short-ranged character of the magnetic interactions. The addition of Al has a negligible effect on the T_C as the localized nature of the magnetic interactions is maintained. It is important to note that although the first-neighbor interaction is very strong, the resulting T_C is quite low. This is due to the fact that for homogeneously distributed spins in a dilute concentration, the probability of having nearest-neighbor spins is very low and, hence, the contribution to the total magnetic interaction is negligible. Only for a high concentration of the magnetic dopants does the short-ranged interactions become important and may result in a true long-ranged ferromagnetic order if magnetic percolation between the dopants is established.

V. CONCLUSION

The absence of remanence in both XMCD and SQUID measurements, together with the results of calculations suggesting that cluster formation is favored, a tendency increasing with Al codoping, leads us to the conclusion that the dominating magnetic behavior in Co:ZnO is superparamagnetic through the formation of antiferromagnetic Co-rich clusters with uncompensated Co spins. Although the Co:ZnO were additionally *n* doped through Al codoping, no ferromagnetism was observed and the superparamagnetic behavior remained unchanged even in case of strong *n* doping as suggested by others.[15] Although structural data indicate phase pure samples, regions rich in Co content cannot be excluded based on our microstructural characterization results. We conclude that the observed magnetism is of superparamagnetic nature due to small AFM clusters of Co atoms with uncompensated surface spins in the ZnO matrix.

ACKNOWLEDGMENTS

We are grateful to Mihela Gorgoi and Svante Svensson for the support during the HIKE measurements at BESSY (Berlin) and to Kjell Jansson at Inorganic Chemistry in Stockholm University for the aid in the TEM studies. Philip Born is acknowledged for the preparation of Co-doped ZnO powder samples. We acknowledge national computational support provided by the SNIC allocation resources in Sweden. Igor A. Abrikosov and Andrei Ruban are gratefully acknowledged for providing the KKR-ASA code to calculate the exchange parameters. The authors are grateful to the Swedish Research Council (VR) and the Knut and Alice Wallenberg Foundation (KAW) for their financial support.

*diana.iusan@fysik.uu.se

[1] T. Jungwirth, K. Y. Wang, J. Mašek, K. W. Edmonds, J. König, J. Sinova, M. Polini, N. A. Goncharuk, A. H. MacDonald, M. Sawicki, A. W. Rushforth, R. P. Campion, L. X. Zhao, C. T. Foxon, and B. L. Gallagher, Phys. Rev. B **72**, 165204 (2005).

[2] G. Chang, E. Kurmaev, D. Boukhvalov, L. Finkelstein, S. Colis, T. Pedersen, A. Moewes, and A. Dinia, Phys. Rev. B **75**, 195215 (2007).

[3] D. Iuşan, B. Sanyal, and O. Eriksson, Phys. Rev. B **74**, 235208 (2006).

[4] K. Sato and H. Katayama-Yoshida, Jpn. J. Appl. Phys., Part 2 **39**, L555 (2000).

[5] C. Song, K. Geng, F. Zeng, X. Wang, Y. Shen, F. Pan, Y. Xie, T. Liu, H. Zhou, and Z. Fan, Phys. Rev. B **73**, 024405 (2006).

[6] S. A. Chambers, Surf. Sci. Rep. **61**, 345 (2006).

[7] J. M. D. Coey, Curr. Opin. Solid State Mater. Sci. **10**, 83 (2006).

[8] P. Sharma, A. Gupta, K. V. Rao, F. J. Owens, R. Sharma, R. Ahuja, J. M. O. Guillen, B. Johansson, and G. A. Gehring, Nat.

Mater. **2**, 673 (2003).
[9] K. Kittilstved, W. Liu, and D. Gamelin, Nat. Mater. **5**, 291 (2006).
[10] A. J. Behan, A. Mokhtari, H. J. Blythe, D. Score, X. H. Xu, J. R. Neal, A. M. Fox, and G. A. Gehring, Phys. Rev. Lett. **100**, 047206 (2008).
[11] X. Liu, E. Shi, Z. Chen, H. Zhang, B. Xiao, and L. Song, Appl. Phys. Lett. **88**, 252503 (2006).
[12] K. Kittilstved, J. Zhao, W. Liu, J. Bryan, D. Schwartz, and D. Gamelin, Appl. Phys. Lett. **89**, 062510 (2006).
[13] K. Kittilstved, D. Schwartz, A. Tuan, S. Heald, S. Chambers, and D. Gamelin, Phys. Rev. Lett. **97**, 037203 (2006).
[14] K. Ueda, H. Tabata, and T. Kawai, Appl. Phys. Lett. **79**, 988 (2001).
[15] P. Sati, C. Deparis, C. Morhain, S. Schafer, and A. Stepanov, Phys. Rev. Lett. **98**, 137204 (2007).
[16] G. Lawes, A. S. Risbud, A. P. Ramirez, and R. Seshadri, Phys. Rev. B **71**, 045201 (2005).
[17] R. Seshadri, Curr. Opin. Solid State Mater. Sci. **9**, 1 (2005).
[18] T. Dietl, H. Ohno, F. Matsukura, J. Cibert, and D. Ferrand, Science **287**, 1019 (2000).
[19] J. M. D. Coey, M. Venkatesan, and C. B. Fitzgerald, Nat. Mater. **4**, 173 (2005).
[20] E. Biegger, M. Fonin, U. Ruediger, N. Janssen, M. Beyer, T. Thomay, R. Bratschitsch, and Y. S. Dedkov, J. Appl. Phys. **101**, 073904 (2007).
[21] B. Sanyal, R. Knut, O. Grånäs, D. M. Iusan, O. Karis, and O. Eriksson, J. Appl. Phys. **103**, 07D131 (2008).
[22] S. Kuroda, N. Nishizawa, K. Takita, M. Mitome, Y. Bando, K. Osuch, and T. Dietl, Nat. Mater. **6**, 440 (2007).
[23] T. Fukushima, K. Sato, H. Katayama-Yoshida, and P. Dederichs, Jpn. J. Appl. Phys., Part 2 **45**, L416 (2006).
[24] K. Sato, T. Fukushima, and H. Katayama-Yoshida, Jpn. J. Appl. Phys., Part 2 **46**, L682 (2007).
[25] C. Pemmaraju, R. Hanafin, T. Archer, H. Braun, and S. Sanvito, arXiv:0801.4945 (unpublished).
[26] A. V. Singh, R. M. Mehra, A. Yoshida, and A. Wakahara, J. Appl. Phys. **95**, 3640 (2004).
[27] J. N. Andersen, O. Björneholm, A. Sandell, R. Nyholm, J. Forsell, L. Thånell, A. Nilsson, and N. Mårtensson, Synchrotron Radiat. News **4**, 15 (1991).
[28] http://www.maxlab.lu.se/beamlines/bld1011/
[29] N. Mårtensson, P. Baltzer, P. Brühwiler, J.-O. Forsell, A. Nilsson, A. Stenborg, and B. Wannberg, J. Electron Spectrosc. Relat. Phenom. **70**, 117 (1994).
[30] M. Gorgoi *et al.*, Nucl. Instrum. Methods (to be published).
[31] G. Kresse and D. Joubert, Phys. Rev. B **59**, 1758 (1999).
[32] G. Kresse and J. Furthmüller, Phys. Rev. B **54**, 11169 (1996).
[33] V. I. Anisimov, F. Aryasetiawan, and A. I. Liechtenstein, J. Phys.: Condens. Matter **9**, 767 (1997).
[34] I. A. Abrikosov and H. L. Skriver, Phys. Rev. B **47**, 16532 (1993).
[35] A. I. Liechtenstein, M. I. Katsnelson, V. P. Antropov, and V. A. Gubanov, J. Magn. Magn. Mater. **67**, 65 (1987).
[36] M. Pajda, J. Kudrnovský, I. Turek, V. Drchal, and P. Bruno, Phys. Rev. B **64**, 174402 (2001).
[37] J. Kudrnovský, I. Turek, V. Drchal, F. Máca, P. Weinberger, and P. Bruno, Phys. Rev. B **69**, 115208 (2004).
[38] L. Bergqvist, O. Eriksson, J. Kudrnovský, V. Drchal, P. Korzhavyi, and I. Turek, Phys. Rev. Lett. **93**, 137202 (2004).
[39] F. Ducastelle, *Order and Phase Stability in Alloys* (North-Holland, Amsterdam, 1991).
[40] M. Kobayashi *et al.*, Phys. Rev. B **72**, 201201 (2005).
[41] S. Krishnamurthy *et al.*, J. Appl. Phys. **99**, 08M111 (2006).
[42] J. Okabayashi *et al.*, J. Appl. Phys. **95**, 3573 (2004).
[43] Z.-X. Shen *et al.*, Phys. Rev. B **42**, 1817 (1990).
[44] G. Carson, M. Nassir, and M. Langell, J. Vac. Sci. Technol. A **14**, 1637 (1996).
[45] J. van Elp, J. L. Wieland, H. Eskes, P. Kuiper, G. A. Sawatzky, F. M. F. de Groot, and T. S. Turner, Phys. Rev. B **44**, 6090 (1991).
[46] S. Hüfner, *Photoelectron Spectroscopy: Principles and Applications*, Advanced Texts in Physics, 3rd ed. (Springer-Verlag, Berlin, 2003).
[47] M. Toyoda, H. Akai, K. Sato, and H. Katayama-Yoshida, Physica B **376-377**, 647 (2006).
[48] X. C. Liu, E. W. Shi, Z. Z. Chen, H. W. Zhang, B. Xiao, and L. X. Song, Appl. Phys. Lett. **88**, 252503 (2006).
[49] L. Neel, C. R. Hebd. Seances Acad. Sci. **252**, 4075 (1961).
[50] T. Dietl, T. Andrearczyk, A. Lipinska, M. Kiecana, M. Tay, and Y. Wu, Phys. Rev. B **76**, 155312 (2007).